JOURNAL OF MATERIALS SCIENCE 37 (2002) 1861 – 1867

Microstructure and hardness of as-cast *in situ* TiB short fibre reinforced Ti-6Al matrix composites

ERLIN ZHANG
National Key Lab. for Precision Hot Processing of Metal, Harbin Institute of Technology, Harbin, 150001, People's Republic of China; Materials Research Department, Risoe National Laboratory, DK-4000, Roskilde, Denmark
E-mail: erlin.zhang@brunel.ac.uk

YUNXUE JIN
National Key Lab. for Precision Hot Processing of Metal, Harbin Institute of Technology, Harbin, 150001, People's Republic of China; Jiamusi University, Jiamusi, People's Republic of China

HONGWEI WANG, SONGYAN ZENG
National Key Lab. for Precision Hot Processing of Metal, Harbin Institute of Technology, Harbin, 150001, People's Republic of China

XD™ technique has been successfully used to prepare TiB short fibre reinforced Ti-6Al matrix composites. Macrostructure and microstructure have been observed by optical microscopy and SEM in order to study the influence of cooling rate on the morphology, size and distribution of TiB. Due to the cooling rate, there exist three kinds of macrostructure: fine grain zone, columnar grain zone and coarse equiaxed grain zone, corresponding to the cooling rate of 100–500 K/s, 20–50 K/s and less than 10 K/s respectively. In the fine grain zone, TiB distributes randomly in matrix with main rod morphology with ~3 μm in width and ~50 μm in length. In the columnar and coarse grain zone, a colony structure was observed in which TiB distributes with a special orientation direction with matrix. A lamellar TiB with up to 50 μm width and 200 μm length was also formed. It was indicated that the decreasing of the cooling rate changes the morphology of TiB from rod to lamellar shape, and markedly increase the length and aspect ration of TiB, from ~50 μm to ~200 μm and from about ~15 to ~200, respectively. TEM results show that the rod TiB has a hexagonal cross section. Vickers hardness testing shows a little reinforcement geometry dependence, but the average hardness of 484 MPa is much higher than that of unreinforced matrix alloy.

1. Introduction

Titanium matrix composites (TMCs) are of interest for high temperature applications. Usually these matrices are reinforced by continuous silicon carbide filaments. However, Three main problems have been identified in SiC/Ti composite materials: (1) the chemical instability between the fibre and the matrix during the processing of the composite material or in service. For example, Ti_3SiC_2, $TiCx$ and $Ti_5Si_3(C)$ reaction products have been observed in the interface between SiC fibre and Ti matrix [1–3]. (2) the tensile residual stresses in the matrix and in the reaction zone due to the coefficient of thermal expansion (CTE) mismatch between the constituents. (3) anisotropic physical and mechanical properties due to the alignment of SiC fibre in the matrix. In order to prevent the reaction, these fibres are coated by a pyrocarbon layer. However, the pyrocarbon layer used on commercial filaments (SCS6 or SM1140) does not change the state of the residual stresses at the interface of SiC/Ti [3]. When the material is submitted to a thermal cycling, these residual stresses must decrease the lifetime of the composite. The efficient way to avoid this chemical reaction is to form the reinforcement by *in situ* precipitation in the titanium matrix [4–9]. The ideal reinforcement should have similar or higher mechanical properties than the silicon carbide (E and UTS) with physical properties (density and CTE) not very far from the matrix. It should also be chemically stable during the processing of the composite. The TiB crystal has a Young's modulus of 550 GPa, a coefficient of thermal expansion of 8.6×10^{-6}/K (quite near to that of titanium, 9.6×10^{-6}/K) and a density of 4.51 kg/cm^3. TiB is considered as one of the best reinforcements for the titanium matrix and widely used in the *in situ* titanium composites research [3].

In the previous researches on *in situ* TMCs, almost all the materials were extruded or forged in order to get a dense materials and good mechanical properties. However, this processing also brought about two main problems: (1) alignment of TiB fibre along the extrusion

direction. This will result in the anisotropic mechanical properties just like that happens in SiC fibre reinforced titanium composites [4, 10]. (2) fracture of TiB fibre, which will introduce pre-crack or crack source in the composites and finally result in the fracture of composites during service [11].

On the other hand, the titanium alloy and their composites are so expensive for mass that they are not suitable for mass production, such as automobile industries. However, casting technology, such as investment casting and permanent casting, is one of the cheapest processes, which provide the possibility to avoid above problems in production of titanium composites.

The present work describes how TiB short fibre reinforced titanium composites is prepared by XD^{TM} *in situ* casting technique. Main purposes were focused on the microstructure and hardness of the as-cast composites, especially the effect of cooling rate on the morphology, size and distribution of reinforcement, and hardness of composites.

2. Experimental procedure

High purity titanium powder (99.7 pct, 45 μm), aluminum powder (99.6 pct, 29 μm) and boron powder (99.8 pct, 45 μm) were dry ball milled for 24 hours. Then they were uniaxially pressed into green compacts and heated in vacuum to synthesize an Al/TiB_2 master alloy. To prepare composites, the master alloy, pure aluminum and the sponge titanium were melted in a water-cooled copper hearth using a non-consumable tungsten electrode. To ensure chemical homogeneity of the melted alloy, electron magnetic agitation was used and the ingots were melted at least three times. Compositions of the composites determined by chemical analysis are listed in Table I. Assumed that B element was completely converted into TiB by the reaction with titanium element, the TiB content is about 6.3 wt%. In order to investigate the effect of the casting condition (cooling rate) on the microstructure and hardness, samples were cut from the ingot longitudinally. Metallographic samples were wet ground with SiC impregnated emery paper using water as the lubricant and subsequently mechanically polished using an alumina-based polishing compound and etched in Kroll's solution. TEM sample was first mechanically polished to 30 μm and thinned by ion-milling. Microstructures were observed on a Philip S-570 scanning electron microscopy (SEM) with energy dispersion spectrum (EDS), and transition electron microscopy (TEM). X-ray diffraction (XRD) analyses were conducted in a Rikagu D/max-RB X-ray diffractometer. The Vickers hardness was measured by LEITZ WETZLAR GERMANY 3940 with 100 g load.

TABLE I Chemical composition of the alloys (wt%)

Alloys	Al	B	O	Ti
Ti-6Al-1.2B	5.33	1.15	0.12	Bal.

3. Results and analyses

3.1. XRD result

Fig. 1 shows the XRD result of Ti-6Al-1.2B alloy. Only diffraction peaks of TiB were found besides that of Ti matrix and no residual TiB_2 or B was found, indicating that they have been completely converted into TiB and only TiB was formed as reinforcement.

TiB is of orthorhombic system. The lattice parameter value a, b and c can be expressed as following:

$$\begin{cases} a = \dfrac{\lambda}{2\sin\theta}\sqrt{H^2 + \left(\dfrac{a}{b}\right)^2 K^2 + \left(\dfrac{a}{c}\right)^2 L^2} \\ b = \dfrac{\lambda}{2\sin\theta}\sqrt{\left(\dfrac{b}{a}\right)^2 H^2 + K^2 + \left(\dfrac{b}{c}\right)^2 L^2} \\ c = \dfrac{\lambda}{2\sin\theta}\sqrt{\left(\dfrac{c}{a}\right)^2 H^2 + \left(\dfrac{c}{b}\right)^2 K^2 + L^2} \end{cases} \quad (1)$$

where θ is Bragge angle. The lattice parameter values associated with each peak position were calculated and plotted as a function of $1/2(\cos^2\theta/\sin\theta + \cos^2\theta/\theta)$ in order to determine the least line as in the following equation:

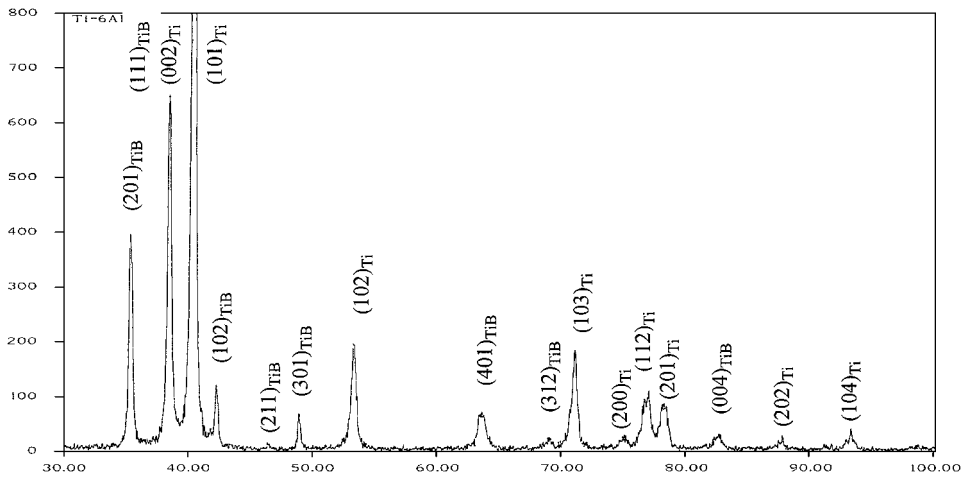

Figure 1 XRD pattern of Ti-6A1-1.2B composites.

TABLE II Normalized X-ray diffraction parameters for TiB peaks

	2θ	d(A)	I	2θ	d(A)	I			
(*hkl*)	In JCPDS			In experiment			a	b	c
(101)	24.481	3.633	20	24.249	3.667	7.14	6.1439	3.0699	4.5756
(200)	29.226	3.053	32	29.143	3.062	23.98	6.1265	3.0633	4.5642
(201)	35.263	2.543	80	35.328	2.539	100	6.1187	3.0584	4.5576
(111)	38.334	2.342	80	38.44	2.34	73.47	6.1064	3.0524	4.5486
(102)	42.192	2.140	100	42.21	2.139	30.61	6.1343	3.0644	4.5679
(211)	46.381	1.956	40	46.32	1.959	4.08	6.1353	3.0671	4.5703
(301)	48.843	1.863	56	48.85	1.863	17.35	6.1260	3.0625	4.5634
(401)	63.634	1.461	28	63.49	1.464	17.35	6.1803	3.0898	4.6040
(312)	68.878	1.362	72	68.86	1.362	7.14	6.1282	3.0630	4.5645

$$\begin{cases} a = a_0 + k_1 \cdot \dfrac{1}{2}\left(\dfrac{\cos^2\theta}{\sin\theta} + \dfrac{\cos^2\theta}{\theta}\right) \\ b = b_0 + k_2 \cdot \dfrac{1}{2}\left(\dfrac{\cos^2\theta}{\sin\theta} + \dfrac{\cos^2\theta}{\theta}\right) \\ c = c_0 + k_3 \cdot \dfrac{1}{2}\left(\dfrac{\cos^2\theta}{\sin\theta} + \dfrac{\cos^2\theta}{\theta}\right) \end{cases} \quad (2)$$

where a_0, b_0 and c_0 are the extrapolated true values of a, b and c when θ approaches 90 degrees and K are the slopes of the least lines.

Table II summaries the X-ray diffraction parameters of TiB. The Lattice parameters calculated from the X-ray diffraction pattern are $a = 6.145$, $b = 3.072$ and $c = 4.577$, respectively, larger than the standard values: $a = 6.123$, $b = 3.060$ and $c = 4.560$, which indicates a shift of diffraction peaks of TiB. In Ti-B binary phase diagram [12], TiB exists in a small composition range of 49–50 at% B. In addition, the thermodynamic calculation has shown that TiB is much stable up to 2400 K with the existence of titanium [13]. So the reason for the shift of the diffraction peak of TiB may be due to the macro-stress concentration caused by solidification in the synthesized TiB reinforcement. Meanwhile, it can also be found that the diffraction peaks of TiB are slightly widened. Considered the large size of TiB analyzed later, it was purposed to be due to the existence of micro-stress concentration in TiB reinforcement.

3.2. Microstructure analyses

Fig. 2 shows the schematic of the macrostructure of the longitudinal section of the composites ingot. Due to the cooling rate, there exist three different macrostructure. From the bottom of the ingot, they are fine (equiaxed) grain zone, columnar grain zone and coarse equiaxed grain zone, respectively. From the other results [14], the cooling rates in the fine (equiaxed) grain zone, the columnar grain zone and the coarse (equiaxed) grain zone are estimated to be 100–500 K/s, 20–50 K/s and less than 10 K/s respectively.

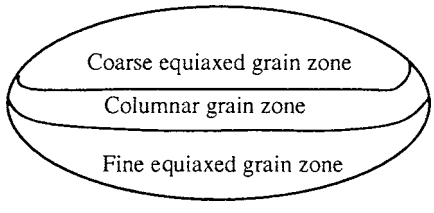

Figure 2 Schematic macrostructure of Ti-6Al-1.2B alloy ingot.

Fig. 3 shows the optical microstructure of Ti-6Al-1.2B alloy at different zones. In the fine grain zone, Fig. 3a and d, the TiB distributes in the matrix homogeneously and isotropically. No special distribution direction can be observed. In the columnar grain zone, shown in Fig. 3b and e, it is found that TiB distributes along the columnar grain direction. In the coarse equiaxed grain zone, a colony structure, which is composed of TiB and Ti, can be observed, as shown in Fig. 3c and f. The space between two TiB fibres is about 2–10 μm. Generally, TiB has only one distribution direction in one matrix grain. However, TiB has different distribution directions at different grains. So the distribution of TiB in macrostructure is still homogeneous and anisotropic, This distribution characteristic is quite different from that of the extruded Ti/TiB composites. In the later case, TiB usually aligns along extrusion direction which will result in the anisotropic mechanical properties as happens in SiC_f reinforced titanium composites [4, 10].

Although the presence of TiB makes it difficult to measure the grain size accurately, the grain size is estimated to be 100–200 μm in the coarse grain zone and less than 50 μm in the fine grain zone. But in the microstructure of *in situ* Ti-6Al/TiC composites produced by the same processing, TiC mainly distributes at the grain boundary, reduces the grain size to 20–30 μm efficiently [5, 6]. It is suggested that some methods should be taken to refine the grain size of matrix in order to get well overall mechanical properties.

As for the reason for the special distribution of TiB, it may be due to the growth characteristics of TiB crystal and solidification characteristics of this alloy. First, the structure of TiB is based on the building block: the trigonal prismatic array of six Ti atoms with a B atom in the center. The TiB structure is formed by closed packing of the trigonal prisms only in one direction, forming columns with a rectangular base with the central chain of B atoms oriented in [101] direction of the crystal. These columns are connected to each other only along the edges, which are parallel to the [101] direction. So TiB is prone to grow with a needle shape. Second, although no Ti-Al-B ternary phase diagram is valued, we still can get some suggestion from Ti-B binary phase diagram. In Ti-B binary phase diagram [12], Ti-1.2%B is a hypoeutectic alloy, so a eutectic structure will be obtained at the end of solidification. During the growth process of this eutectoid, because

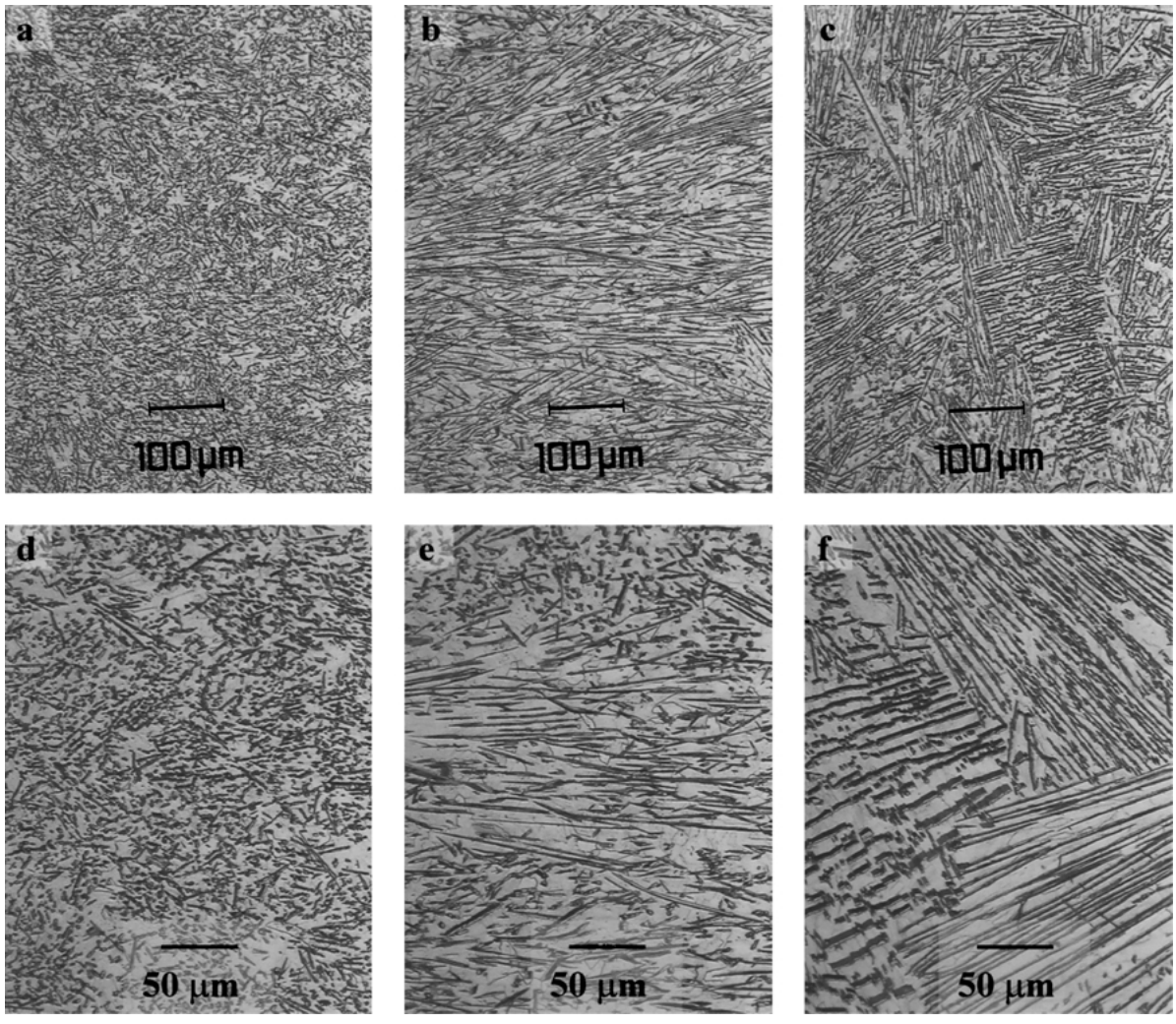

Figure 3 Optical microstructure of Ti-6A1-1.2B alloy. (a) and (d) microstructure of the fine grain zone, (b) and (e) microstructure of the columnar grain zone, (c) and (f) microstructure of the coarse equiaxed grain zone.

TiB content is less than 30%, it will grow with Ti matrix in a co-growth growth model [15]. Some researches [16–19] indicate those TiB forms as whiskers or fibres with high aspect ratio with the orientation relationships between TiB and α-Ti as described by

$(010)_{TiB}$// $\{1120\}_{Ti}$ and $\langle 102\rangle_{TiB}$//$[0001]_{Ti}$
and
(010)// $\{1210\}_{Ti}$ and $\langle 001\rangle_{TiB}$//$[0011]_{Ti}$
and
(010)//$\{1120\}_{Ti}$ and $\langle 001\rangle_{TiB}$//$[0001]_{Ti}$

with the $[010]_{TiB}$ direction parallel to the axis of the fibres. A common feature in the above three orientation relationships is that they contain the same element: (010)//$\{1120\}_{Ti}$ or $[010]_{TiB}$//$\{1120\}_{Ti}$. It seems that there is no fixed orientation relationship between TiB and Ti, except (010)//$\{1120\}_{Ti}$ or $[010]_{TiB}$//$\{1120\}_{Ti}$. In other words, the direction $[010]_{TiB}$ is always parallel to the direction of $\langle 1120\rangle_{Ti}$. However, both TiB and Ti can rotate along this common axis with respect to each other. According to this peculiar orientation relationship, there will be three possible variant directions for TiB fibre in a single Ti crystal, depending on $[010]_{TiB}$ parallel to which $\langle 1120\rangle_{Ti}$, and each variant will have an angle of 60° with the other two variants. As a result, TiB in one grain will distribute with one of above three orientation relationships with matrix grain, and have different distribution directions in different Ti grains, as observed in the columnar and coarse grain zone. However, in the fine grain zone, because the grain is so small that it is difficult to observe this kind of distribution characteristic by optical microscopy and SEM.

Fig. 4 shows the morphology of TiB in different zones observed by SEM. In the fine grain zone (Fig. 4a and b), TiB is mainly of rod shape with less than 50 μm in length and 3 μm in width. In the columnar grain zone, Fig. 4c and d, some long lamellar TiB are also found beside rod shape TiB. The length of TiB becomes much longer than that in the fine grain zone, about 100–200 μm. In the coarse grain zone, Fig. 4e and f, almost all TiB are of lamellar shape with up to 50 μm in width and 100–200 μm in length, only a few TiB is still in rod shape. Table III summarizes the microstructural parameters of TiB. From above results, it can be found that with the decreasing of cooling rate, the shape of TiB changes from rod shape to lamellar shape. Meanwhile, the length and aspect ratio increase from ~50 μm to ~200 μm and from about ~15 to ~200, respectively.

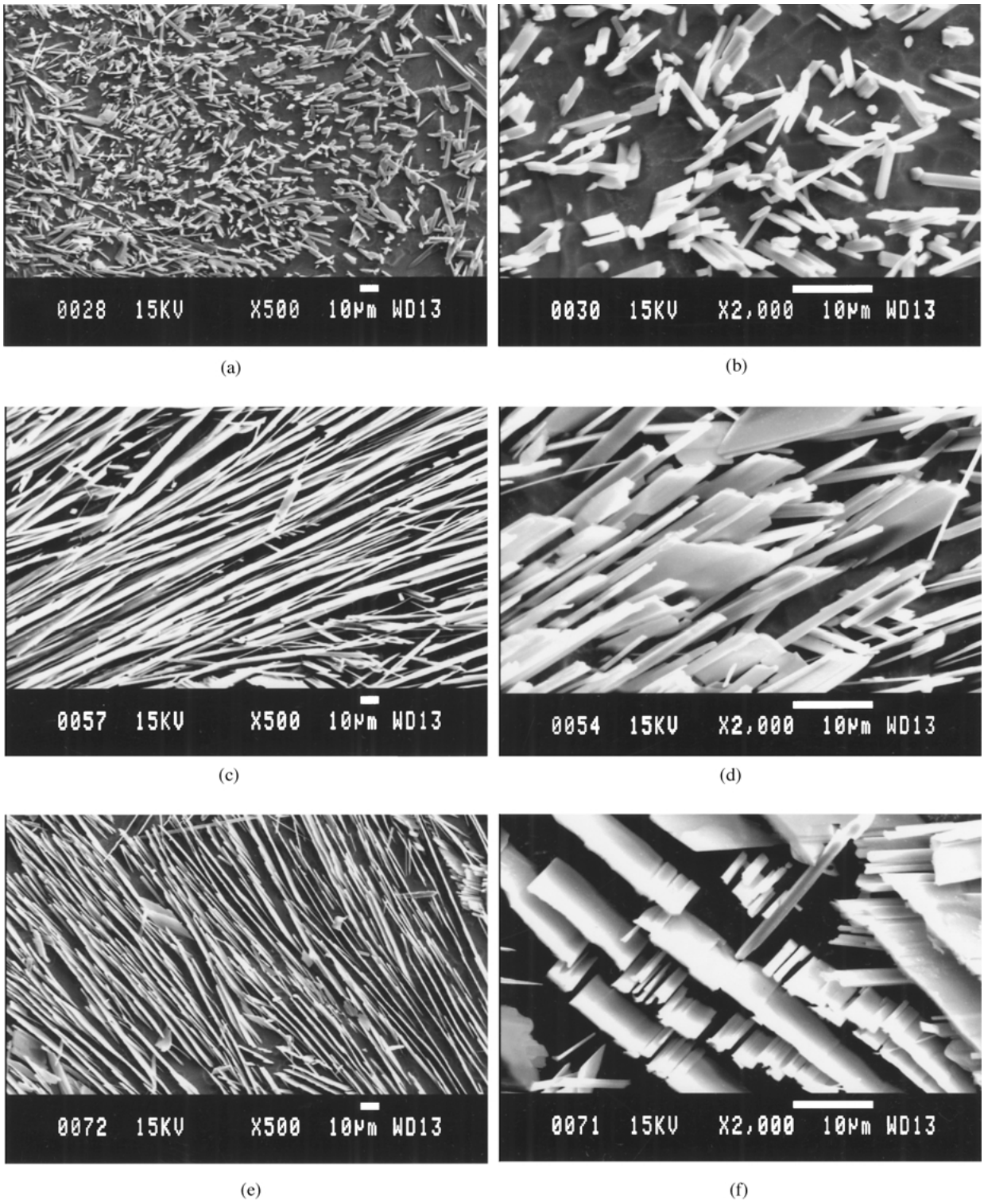

Figure 4 Morphology of TiB in different zone of Ti-6Al-1.2B alloy ingot. (a) and (b) fine grain zone, (c) and (d) columnar grain zone, (e) and (f) coarse equiaxed grain zone.

TABLE III Summary of microstructural parameters of TiB fibres

Position	Cooling rate (K/s)	TiB short fibre			
		Morphology	Width (μm)	Length (μm)	Aspect ratio
Fine grain zone	100–500	Rod	~3	~50	~15
Columnar grain zone	20–50	Rod, lamellar	~20	~200	~200
Coarse equiaxed grain zone	<10	Lamellar, rod	~50	~200	~200

Fig. 5 shows TEM morphology of the cross section of fine rod TiB fibres. A hexagonal section can be clearly seen. In addition, it also reveals that a clean interface exists between the *in situ* TiB and titanium matrix.

3.3. Hardness measurement

Fig. 6 shows the change of the Vickers hardness of the composites along the longitudinal direction with the distance from the sample bottom.

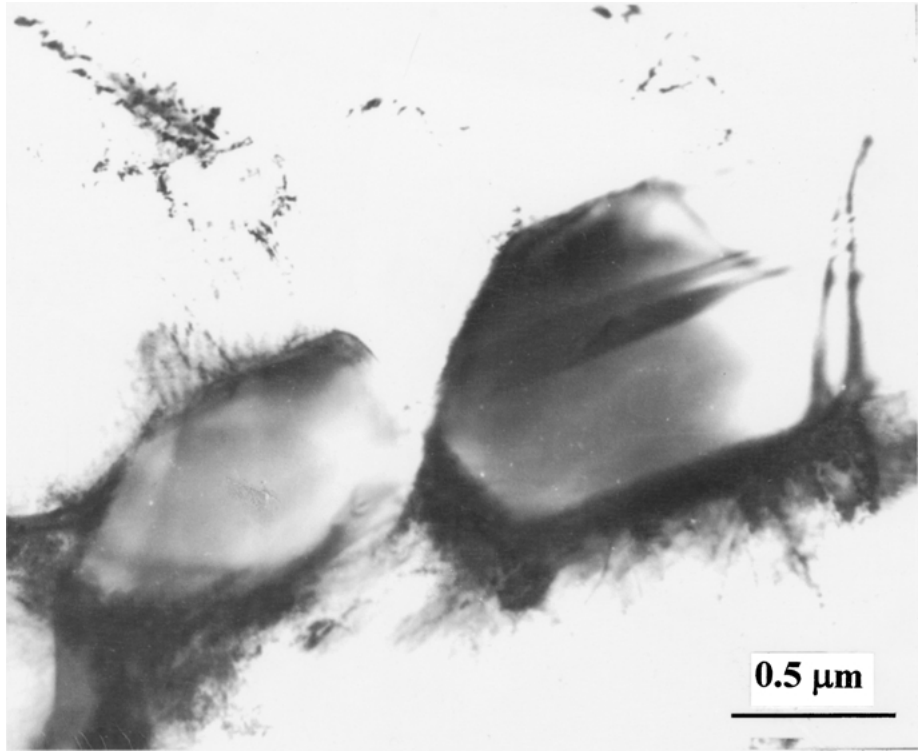

Figure 5 TEM microstructure of rod shape TiB fibre in as-cast *in situ* Ti-6Al-1.2B composites.

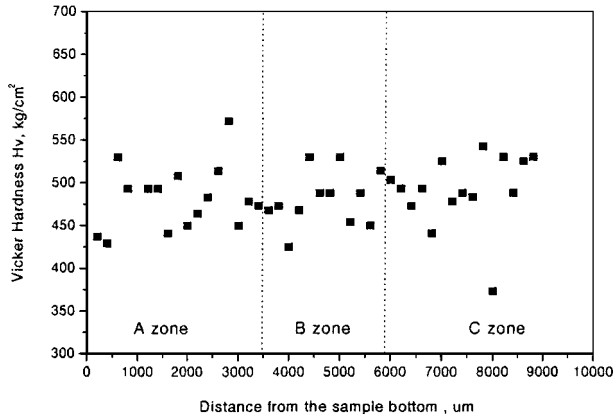

Figure 6 Change of the Vickers hardness of the composites along the longitudinal direction with the distance from the sample bottom. A, B, and C zone in the figure represent the fine grain zone, the columnar grain zone and the coarse grain zone, respectively.

The average hardness in the fine grain zone, the columnar grain zone and the coarse grain zone are 481 kg/cm^2, 481 kg/cm^2 and 491 kg/cm^2, respectively. Although there is large difference in the microstructure of these three zones, only a 10 kg/cm^2 increase in hardness can be found in the coarse grain zone, suggesting that a little dependence of hardness on reinforcement geometry. However, the average Vickers hardness of this alloy is as high as 484 kg/cm^2, much higher than that of unreinforced Ti-6Al alloy (274 kg/cm^2) [6], indicating that the formation of TiB fibre reinforcement markedly increases the hardness, about 76.6% increase.

4. Conclusion

(1) The cooling rate has great influence on the distribution of TiB reinforcement. With the decreasing of cooling rate, the distribution of TiB changes from random distribution in all grain to regular distribution in one grain. However, the distribution of TiB reinforcement in the matrix is still homogeneous and isotropic in macrostructure.

(2) The cooling rate also has large influence on the morphology and size of TiB reinforcement. With the decreasing of cooling rate, the morphology of TiB changes from rod shape to wide lamellar shape. Meanwhile, the size and aspect ratio increase with the decreasing cooling rate.

(3) Hardness testing results show a little reinforcement geometry dependence of hardness of composites. However, the average hardness of 484 kg/cm^2 is much higher than that of unreinforced matrix alloy, 76.6% increase.

Acknowledgement

This program is supported by the Foundation of National Key Lab. for Precision Hot Processing of Metal of China (99JS61.5.1.ZS6102).

References

1. S. GORSSE and Y. LE PETITCORPS, *Composites* part A **29A** (1998) 1221.
2. R. J. KERANS, K. S. MAZEIYASHI, R. RUI and H. A. LIPSITT, *J. Amer. Ceram. Soc.* **67** (1984) 34.
3. S. GORSSE, J. P. CHAMINADE and Y. LE PETITCORPS, *Composites* part A **29A** (1998) 1229.
4. Z. Y. MA, S. C. TIONG and L. GEN, *Script Materialia* **42** (2000) 367.
5. ZHANG ERLIN, JIN YUNXUE, ZENG SONGYAN and ZHU ZHAOJUN, *Transaction of Non-Ferrous Metal Society* **10**(6) (2000) 764.
6. ZHANG ERLIN, ZENG SONGYAN and ZHU ZHAOJUN, *J. Mater. Sci.* **35** (2000) 5989.
7. D. X. LI, D. H. PING, Y. X. LU and H. Q. HE, *Mater. Letter* **16** (1993) 322.

8. L. WANG, M. NIINAOMI, S. TAKAHASHI, M. HAGIWARA, S. EMURA, Y. KAWABEI and S. J. KIM, *Mater. Sci. Eng*. **A263** (1999) 319.
9. S. S. SAHAY, K. S. RAVICHANDRAN, R. ATRI, B. CHEN and J. RUBIN, *J. Mater. Res*. **12** (1999) 4214.
10. FENG TANG, S. EMURA and M. HAGIWARA, *Scripta Mater*. **43** (2000) 573.
11. H. T. TSANG, C. G. CHAO and C. Y. MA, *ibid*. **35** (1996) 1007.
12. T. B. MASSALSKI (Ed), "Binary Alloy Phase Diagram" (The Materials Information Society, 1990).
13. XIAONONG ZHANG, WEIJIE LU, DI ZHANG and RENJIU WU, *Scripta Mater*. **41** (1999) 39.
14. N. H. PRYDS, unpublished report, Dec. 2000.
15. LI CHAO (Ed), "Theory of Metallography" (Harbin Institute of Technology Press, Harbin, 1990).
16. Z. FAN, Z. X. GUO and B. CANTOR, *Composites* **28A** (1997) 131.
17. T. YAMANOTO, A. OTSUKI, K. ISHIHARA and P. H. SHINGU, *Mater. Sci. Eng*. **A239/240** (1997) 647.
18. S. S. SAHAY, K. S. RAVICHANDRAN and R. ATRI, *J. Mater. Res*. **14** (1999) 4214.
19. M. E. HYMAN, C. MCCULLOUGH, J. J. VALLENCIA, C. G. LEVI and R. MEHRABIAN, *Metall. Trans*. **20A** (1989) 1847.

Received 14 February
and accepted 11 December 2001